Meter-scale geologic heterogeneity in the near surface explains seismic speckle scattering noise

Andrey Bakulin[1], Ahmad Ramdani[2], Dmitry Neklyudov[3], and Ilya Silvestrov[1]

https://doi.org/10.1190/tle42100683.1

Abstract

Complex scattering in the near surface can introduce significant distortions in deep reflection data. To model and explain these effects, a multiplicative random noise model based on the speckle mechanism of small-scale scattering has been proposed. While this model effectively captures the observed phenomena in field data, it has been considered rather abstract as it relies on random mathematical clutter to replicate the distortions. This study goes beyond by delving into the analysis of the actual meter-scale geologic heterogeneity found in carbonate formations from desert environments. By employing elastic wave propagation simulations, we show that geologic heterogeneity is equally capable of generating the observed speckle noise in field data when compared to idealized mathematical clutter. Our simulations reveal that the phase perturbations exhibit a quasi-random nature and follow a symmetric near-normal distribution, thereby supporting the validity of the multiplicative noise model and aligning with field observations. Furthermore, we discover that the spread or standard deviation of phase perturbations increases with frequency. This finding provides a plausible explanation for the loss of higher frequencies commonly seen in our data. By considering the complex waveform distortions induced by near-surface heterogeneity, our new noise model represents a significant advancement over residual statics that only account for the kinematic aspect. In summary, our study shows that geologic heterogeneity can easily generate the speckle noise observed in field data. The complex waveform distortions can be captured using quasi-random phase perturbations, as the multiplicative noise model outlines. This advancement leads to a more comprehensive understanding of the influence of near-surface heterogeneity on seismic data. Consequently, this understanding serves as a foundation for despeckling deep reflection data and enhancing the resolution of seismic imaging. These findings have significant implications for improving the quality and accuracy of seismic imaging in areas where speckle noise dominates.

Introduction

Challenging seismic data can arise in specific geologic environments. A prominent example is data obtained from desert environments in the Middle East. Reflections are often overwhelmed by intense near-surface arrivals such as ground roll. They further exhibit low coherency and variable wavelets caused by strong heterogeneity. The complex near surface is often assumed to be responsible for this phenomenon (Ait-Messaoud et al., 2005; Bridle et al., 2006; Vesnaver, 2006; Bakulin and Silvestrov, 2021). Prestack seismic data with small arrays and single sensors can be particularly challenging to process (Bakulin et al., 2020, 2022). The presence of medium- and small-scale heterogeneity has long been recognized as a major contributing factor to the complexity of land seismic data (Bakulin et al., 2016, 2022; He et al., 2017; Stork, 2020). However, no specific mechanisms have been identified to explain the severe reflection distortions observed in these complex data. Even deep reflectors that do not directly interfere with near-surface arrivals frequently exhibit chaotic and disrupted characteristics, rendering them challenging to analyze and explore for deeper targets. Bakulin et al. (2022) introduced a multiplicative random noise model for speckle scattering noise that could plausibly explain the most complex distortions seen on the field data. This model connects distortions seen in the data with statistical properties of the small-scale heterogeneity and draws upon an existing understanding of speckle noise in various fields, including optics and acoustics (Goodman, 2020). The statistical nature of the model acknowledges the inherent challenge of capturing the deterministic behavior of the small-scale heterogeneity responsible for these distortions. Bakulin et al. (2020, 2022) utilized a mathematical model of random clutter as a substitute for a complex near-surface scattering layer and successfully reproduced key characteristics observed in field data. However, there was still a debate regarding whether actual geologic heterogeneity could exhibit the required random-like characteristics and possess the necessary geometric and elastic properties to accurately reproduce speckle scattering noise. Recently, advancements in characterizing meter-scale geologic heterogeneity in desert environments (Vahrencamp et al., 2019; Ramdani et al., 2022a, 2022b, 2022c) have addressed this gap and provided actual near-surface models that can serve as a foundation for further analysis.

This research establishes a crucial connection between realistic geologic models incorporating meter-scale heterogeneity and the generation of speckle noise. It achieves this through synthetic elastic modeling and comparison with field data, demonstrating the ability to produce speckle noise characterized by random, frequency-dependent phase distortions that resemble real field observations.

Once this core relationship between geology and speckle noise is established, strategies for noise mitigation can be developed. Advanced techniques like seismic time-frequency masking (Bakulin et al., 2023) can despeckle deep reflection data. This study aims to provide foundational justification for such approaches based on geologic factors — a unique contribution in geophysical literature.

[1]Saudi Aramco, EXPEC Advanced Research Center, Dhahran, Saudi Arabia. E-mail: a_bakulin@yahoo.com; ilya.silvestrov@aramco.com.
[2]Ali Al-Naimi Petroleum Engineering Research Center, King Abdullah University of Science and Technology, Saudi Arabia. E-mail: ahmad.ramdani@kaust.edu.sa.
[3]Institute of Petroleum Geology and Geophysics SB RAS, Novosibirsk, Russia. E-mail: dmitn@mail.ru.

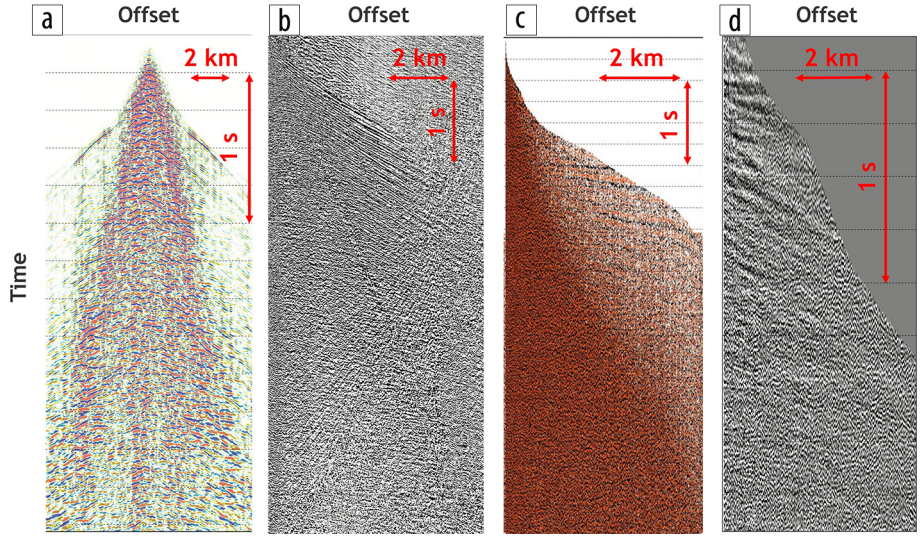

Figure 1. Prestack gathers from different scattering areas: (a) crosspread gather from area A; (b) common-depth-point (CDP) gather from area B; (c) CDP gather from area C; and (d) CDP gather from area D. Data in (a)–(c) were acquired with nine-geophone arrays, whereas (d) correspond to single-sensor data. All gathers are shown after the removal of linear and spiking noise.

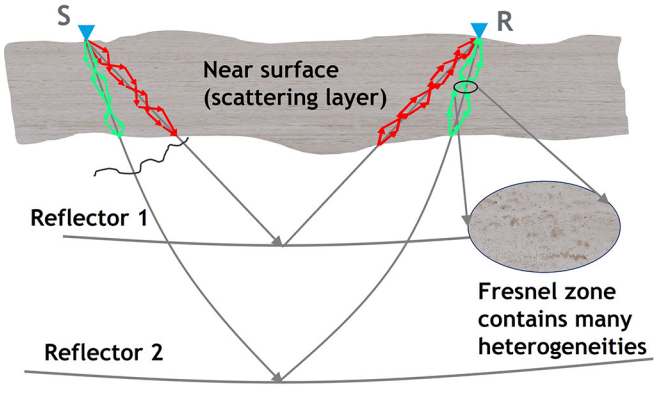

Figure 2. Diagram depicting the source of reflection distortions caused by speckle scattering noise. Unlike the homogeneous scenario with a single arrival, the combination of multiple forward-scattering arrivals creates an intricate interference pattern, resulting in altered phase and amplitude rapidly changing from trace to trace.

This rationale holds particular significance for deep exploration, as it establishes the groundwork for innovative despeckling tools that extend beyond just improving near-surface models. The research introduces a meter-scale model to validate speckle-inducing effects in actual near-surface geology alongside mathematical representations of random multiplicative noise. However, generating such models routinely for deep exploration is unfeasible. Consequently, mitigating noise in deep reflection data hinges on statistical techniques heavily influenced by the speckle noise model.

Field data from geologic environments with scattering speckle noise

Figure 1 presents field data from four distinct and complex desert environment areas arranged to exhibit rising levels of complexity. The lower sections of the collected data correspond to depths of 3–6 km, which are common in deep exploration. The initial three data sets correspond to high-channel-count acquisition geometry employing nine-geophone arrays (Dmitriev et al., 2017), as shown in Figures 1a–1c. The fourth data set is from a single-sensor acquisition (Cordery, 2020), which is illustrated in Figure 1d. All the presented data sets have undergone initial preprocessing that removed linear and spiking noise. In addition, the single-sensor data set has undergone surface-consistent processing. Notably, we can observe distinct and characteristic speckle-type noise, which is believed to be a result of near-surface scattering (Bakulin et al., 2022). This noise presents itself as fragmented reflection events with varying waveforms. Seismic processing techniques generally operate under the assumption that noise is superimposed onto the underlying signal. Therefore, the primary goal is to remove the noise and uncover the original signal, presuming it is otherwise unaffected.

Bakulin et al. (2022) argue that these effects, observed in land seismic data, occur in intricate near-surface conditions and cannot be solely attributed to additive noise. Instead, they introduced the notion of speckle seismic noise, a distinct type of noise-resembling phenomena observed in optics and acoustics. Figure 2 illustrates how speckle noise is generated in seismic data. The wavefield interacts with closely spaced heterogeneities that are smaller than the seismic wavelength. Instead of a single arrival as expected in homogeneous media, this interaction gives rise to the interference of multiple near-ballistic arrivals in the seismic data. This interference alters the phase and amplitude of the resulting wave packet, creating a distinct speckle-like appearance.

In contrast to additive noise, speckle noise is described by a random multiplicative model (Goodman, 2020; Bakulin et al., 2022). To illustrate the differences, the general seismic trace model that includes both multiplicative and additive noise can be written as:

$$x_k(t) = r_k(t) * s(t) + n_k(t), \quad (1)$$

where $s(t)$ is the clean signal, $r_k(t)$ is a random multiplicative noise term describing signal distortion, $n_k(t)$ is additive random noise, $*$ denotes convolution, and k is a trace or channel number. In the context of Figure 2, the term "clean signal" refers to the wavefield that would be recorded if all small-scale heterogeneities in the near-surface layer were removed. The multiplicative model is not a new concept in geophysics and has been used to describe surface-consistent deconvolution (Cary and Lorentz, 1993). However, it was not previously used to describe random speckle noise in seismic data, as is commonly done in optics and acoustics (Goodman, 2020). It is important to highlight several key differences between multiplicative and additive noise:

- Multiplicative noise is induced by the signal itself, reflecting its scattering nature. If there is no signal, there is no multiplicative noise. In contrast, additive noise can be recorded and analyzed even in the absence of the signal. However, recording and analyzing multiplicative noise without a signal is impossible.
- Multiplicative noise distorts reflection events and other arrivals, leading to fragmented appearances and diminished coherency.
- Multiplicative noise impacts both strong and weak signals proportionately, leading to distortion that scales with the signal size. On the other hand, additive noise is not influenced by signal strength.

Small-scale heterogeneities that give rise to speckle seismic noise are often challenging to characterize deterministically. In simple terms, constructing a migration velocity model that effectively captures these fine-scale features using data-driven workflows is not possible. Nevertheless, if such a model could be achieved, migration could be employed to mitigate a major part of speckle distortions in imaging. Consequently, statistical techniques to attenuate random multiplicative noise are the most practical approach for handling this type of noise in seismic data.

Bakulin et al. (2022) proposed a simplified model of multiplicative seismic random noise formulated in the frequency domain and inspired by prior speckle studies from other fields. Equation 1 can be rewritten in the Fourier domain as:

$$X_k(\omega) = R_k(\omega)S(\omega) + N_k(\omega), \tag{2}$$

where X_k, R_k, S, and N_k are Fourier transforms of the corresponding time-domain functions in equation 1. The speckle noise model proposes that there are random, frequency-dependent phase fluctuations $\varphi_k(\omega)$, leading to the following noise term:

$$R_k(\omega) = e^{i\varphi_k(\omega)}. \tag{3}$$

The scenario in which phase perturbations $\varphi_k(\omega)$ exhibit random variations across frequencies within a given channel is classified as *the first type of multiplicative random noise with random frequency–dependent phase fluctuations*. Bakulin et al. (2022) also demonstrated that the well-known phenomenon of residual statics can be interpreted as a *second type of multiplicative noise*. In this case, for a specific channel, $\varphi_k(\omega)$ represents a deterministic linear function derived from a fixed time delay value. As the scenario progresses, the next channel introduces a different random time shift value, resulting in the definition of another linearly varying function, $\varphi_{k+1}(\omega)$, and so forth. Bakulin et al. (2022) demonstrated that the combined effect of two multiplicative noises could consistently explain crucial field observations based on data from scattering environments:

1) Even after advanced processing, prestack reflections remain distorted with low coherency and are challenging to track. Furthermore, these distortions are not localized but distributed throughout the entire data set, making it difficult even to pick first breaks or use early arrivals for full-waveform inversion.
2) Applying local stacking improves the visibility of reflections, but the absolute level of amplitude spectra is significantly biased downward across all frequencies.
3) Amplitude spectra show increasing attenuation with frequency as a result of local stacking.

Assuming Gaussian-distributed phase fluctuations with a consistent spread or standard deviation across frequencies explains two important observations. First, it remarkably and accurately reproduces the observed data scrambling (first observation). Second, it provides a compelling rationale for amplitude reduction during stacking (second observation). Residual statics were solely required to account for the progressive loss of higher frequencies, as noted in the third observation. Bakulin et al. (2022) additionally pointed out that if the spread or standard deviation increases with frequency for the first type of noise, it can also explain the gradual loss of higher frequencies observed after local stacking. Therefore, all three observations can be adequately explained without needing to consider residual statics as an explanatory factor.

We will break down the process of linking speckle noise that affects deep reflectors and meter-scale geologic near-surface heterogeneity into three steps. First, we examine whether realistic geologic models of near-surface layers can faithfully reproduce the observed reflection distortions seen in field data, shown in Figure 1. Second, we evaluate the effectiveness of proposed mathematical models in describing these distortions and determine which ones are best for this job. Lastly, we gain insight into how phase changes with frequency by comparing field data with synthetic data generated using realistic geologic models.

Field data

Before we begin the modeling exercise, it is important to provide a reference for the behavior of the real data. Figure 3a shows a challenging deep portion (below 4 km) of prestack gathers after preprocessing. In this section, all reflectors are severely cluttered and barely discernible. However, after local stacking with nonlinear beamforming (Bakulin et al., 2018), most of the events become detectable (Figure 3b). This suggests that signals are present in Figure 3a but are subject to severe distortions that prevent their detection. Figures 3c–3e exhibit a smaller 200 ms subwindow limited to near-mid offsets. Figure 3c highlights the difficulty of deep exploration, where prestack reflector identification alone is a challenge. Local stacking (Figure 3d) restores coherence by rectifying the phase, yet it leads to dampened higher frequencies and excessively smoothed amplitude characteristics (Bakulin et al., 2022). Lastly, Figure 3e presents the despeckled outcome through seismic time-frequency masking (Bakulin et al., 2023), addressing amplitude noise with the lighter touch using local stacking as a guide.

Figures 4a and 4b contrast the original and beamformed data phase from Figures 3c and 3d. It is important to mention that the phase of the data after despeckling using seismic time-frequency masking (Figure 3e) matches that of the locally stacked data, so it has been omitted. The beamformed data have a more continuous phase, consistent with our visual perception of coherent and trackable events. In contrast, the phase of the original data

randomly oscillates around the beamformed phase. If we were to analyze the difference between the two phases (Figures 4c and 4d), we would observe a symmetrical Gaussian-like distribution, similar to what the theoretical noise model postulates. The randomized phase is a typical component of speckle modeling (Goodman, 2020), and the presented figures demonstrate that randomization leads to a loss of coherence, similar to what is observed in the field data in Figure 1. Data also suggest that spread or standard deviation tends to increase with frequency (compare Figures 4c and 4d). The significance of this finding lies in its ability to potentially explain the progressive loss of higher frequencies, as mentioned in the third observation, without the need for residual statics.

Previous studies have replicated the field-like behavior of gathers and phases using an acoustic model with random mathematical clutter as a near-surface scattering layer (Bakulin et al., 2020, 2021, 2022). In the following section, we will evaluate the properties of the elastic wavefield in models with realistic geologic heterogeneity.

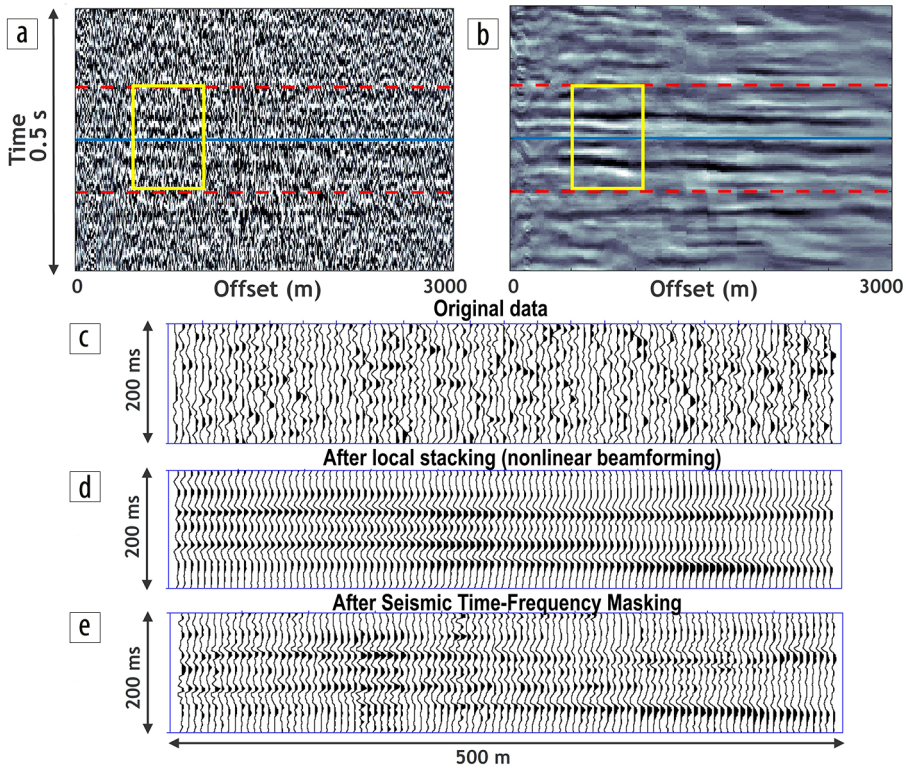

Figure 3. In a deep portion of the data, a prestack window reveals highly cluttered reflectors: (a) prestack CDP gather after conventional processing; (b) same as (a) but after local stacking with nonlinear beamforming. The improved coherency of all the horizontal reflection events is evident, although it comes at the cost of spatial smearing and the loss of higher frequencies. Zooming in on a smaller subwindow (indicated by the yellow box) reveals: (c) original data with complex distortions; (d) data after local stacking, showing the balance between improved coherency and excessive smoothing; and (e) data after advanced despeckling using seismic time-frequency masking, demonstrating improved coherency while preserving higher frequencies and amplitude characteristics (Bakulin et al. 2023). All data are shown after normal moveout corrections.

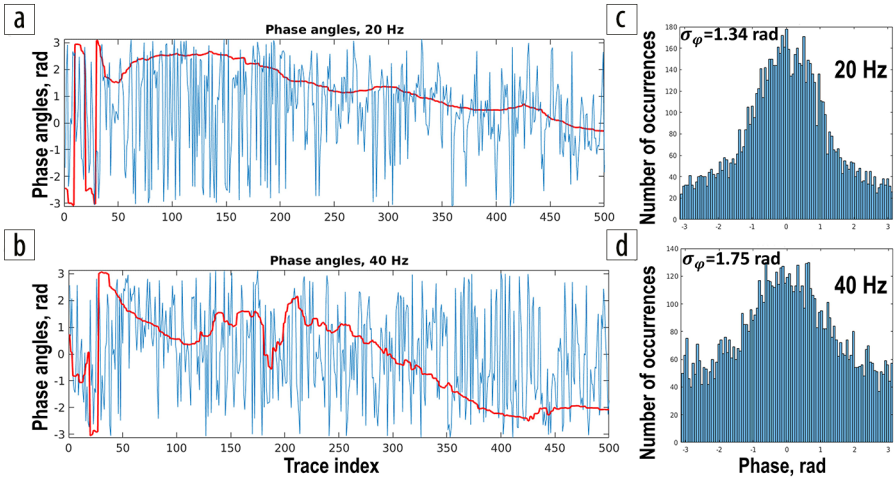

Figure 4. Phase calculated in the smaller subwindow (shown in Figures 3c–3d) for (a) 20 Hz and (b) 40 Hz. The phase of the raw data is depicted in blue, while the locally stacked data are shown in red. Histograms of the wrapped phase difference between the original and beamformed data (residual phase) are shown in (c) and (d). Notice the wider phase spread at (d) 40 Hz compared to (c) 20 Hz. Note that the phase following seismic time-frequency masking (as depicted in Figure 3d) is the same as the one obtained through local stacking and is therefore not displayed. For consistency with model definition (3), standard deviations for the unwrapped phase are posted on the plots.

Synthetic data generated from realistic geologic modeling of meter-scale near-surface heterogeneity

Carbonate rocks are intrinsically heterogeneous at a multiscale level (Eberli et al., 2003; Borgomano et al., 2013; Ramdani et al., 2022c). An interplay between sedimentary fabric, lateral and vertical depositional facies changes, overprinting diagenesis, and fracture distribution contributes to the 3D meter-scale heterogeneity of petrophysical properties in carbonate formations (Vahrenkamp et al., 2019; Ramdani et al., 2023). Among these factors, the distribution and morphology of skeletal bioconstructed geobodies are the most heterogenous depositional facies contributor in the carbonate strata (Al-Mojel et al., 2020; Ramdani et al., 2022b). The abstract concepts of speckle noise, especially on the near surface of Arabia, may be explained by the presence of these facies. Outcrop studies and near-surface petrophysical properties measurements of the Late Jurassic stromatoporoid-coral buildup complex in Arabia conceivably support this understanding (Ramdani et al., 2022a; Ramdani et al., 2022c). As a result, we closely examine this current geologic understanding

and simulate its synthetic responses to substantiate the genuine geologic origin of speckle noise.

Geologic modeling. Outcrop studies (Al-Mojel et al., 2020; Ramdani et al., 2022c) reveal that the Late Jurassic Arabian stromatoporoid-coral buildup facies appear patchy on the kilometer-size outcrop scale, occupying an approximate 10%–20% proportion of the strata. They also exhibit hierarchical scaling relationships where smaller buildup units and their associated flank congregate into larger clusters with amalgamated pseudo-ellipsoid morphology (Figures 5a and 5b). Accommodation space at each parasequence controls the lateral and vertical growth of these buildup complexes. The growth of these buildups may be simplified into four distinct process-based stages (Ramdani et al., 2022c): initiation, congregation, maximum growth, and termination (Figure 5c). In this study, we performed a 2D process-based geologic facies modeling to replicate the scaling relationship and growth pattern of the Late Jurassic Arabian stromatoporoid-coral buildups. This modeling workflow is a simplified 2D version of a more comprehensive modeling methodology described in Ramdani et al. (2022c).

We constructed two models, representing two different buildup-hosting strata (Figure 6f). Model 1 is 6000 m long and has a 40 m thick buildup zone. Model 2 has a similar length with a 120 m thick buildup zone. The models were constructed by first recreating the overall morphology of the buildup clusters and their flanks as ellipsoidal polylines vertically constrained by modeled stratigraphic surfaces (Figure 5c). A set of buildup nucleation points are distributed throughout the models. A 2D ellipsoid was constructed from each nucleation point, and buildup ellipsoids that grew within the approximately 60 m clustering distance assembled into larger buildup clusters mimicking the initiation and congregation stage. The number of nucleation points, clustering distance, buildup length, and buildup thickness distributions were sampled from outcrop studies by Ramdani et al. (2022c). Provided enough accommodation space, the buildup clusters in the next stratigraphic block were constructed on top of the previous buildup in a backstepping manner simulating the maximum growth stage. Finally, we arranged the buildup ellipsoids at the termination stage in a prograding manner to simulate the limited accommodation space.

We constructed the facies and elastic property models by converting the buildup polylines into geocellular grids (Figures 5d and 5e). The resulting polylines were sampled into 3 m × 30 cm 2D geocellular grids where two facies schematics were assigned: the buildups and background strata (Figures 5d and 5e). The resulting models contained approximately 10%–20% of buildup facies with an average of approximately 14% (Figure 6a). The buildup facies also had length and thickness distributions that were relatively consistent (Figures 6b and 6c) with outcrop

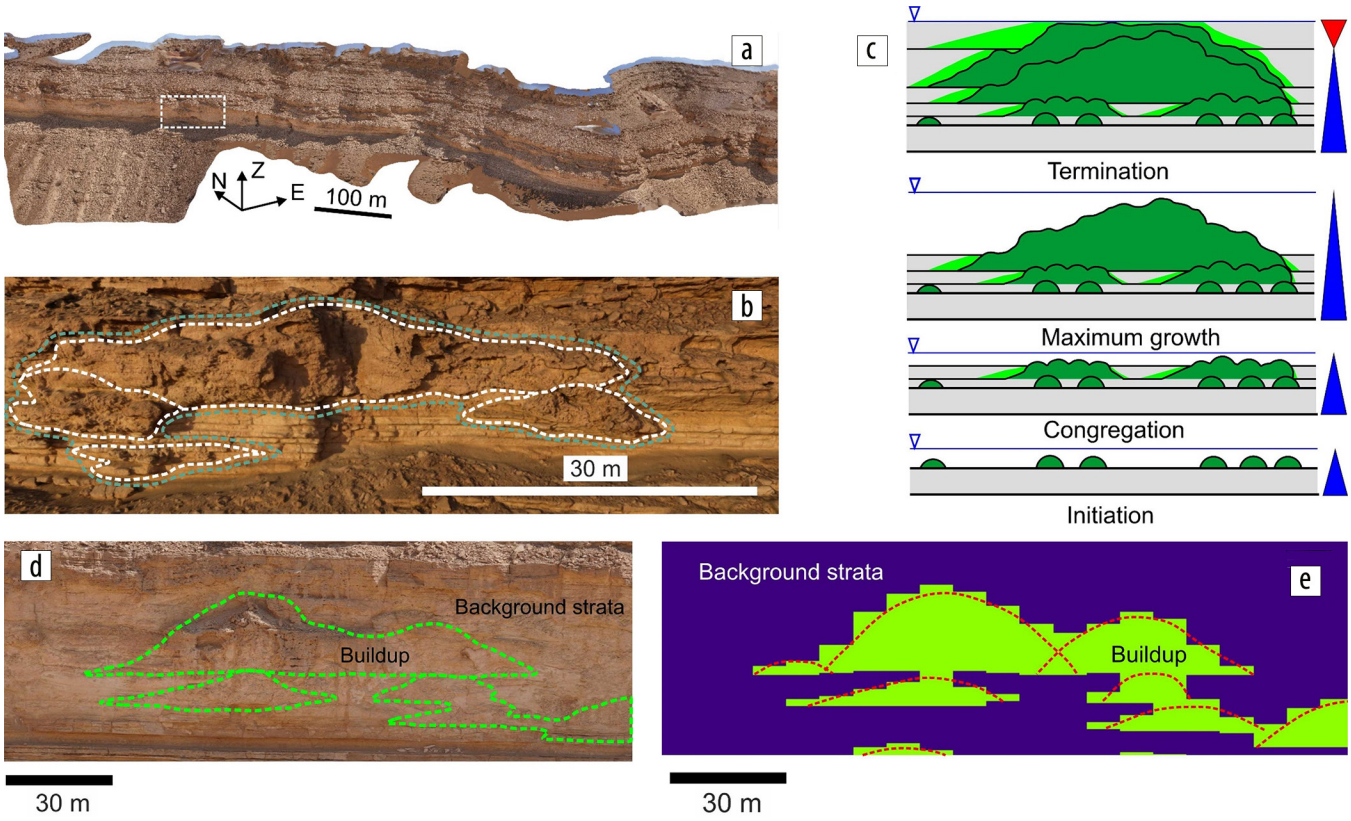

Figure 5. (a) Example of a digital outcrop model showcasing the stromatoporoid-coral buildup facies found in the Arabian Late Jurassic Carbonate strata. The dashed polygon indicates a zoomed-in location of a cluster of buildups, as depicted in Figure 5b. (b) Cluster of stromatoporoid-coral buildups, consisting of numerous smaller buildups. The buildups are identified in the outcrop as weathering-resistant features that appear bulbous and chaotic, devoid of any clear bedding compared to the background strata. (c) Conceptual four-stage process-based model illustrating the growth and lateral extent of the buildups. This model serves as the foundation for constructing the facies model in this study. Figures 5a–5c have been adapted from Ramdani et al. (2022c). (d) Example of the resulting 2D buildup polylines (dashed line) overlaid onto the digital outcrop model. Notably, the model accurately delineates the boundaries of the buildups observed in the outcrop. (e) Facies model derived from sampling the polylines depicted in Figure 5d and incorporating them into geocellular grids.

observation reported by Ramdani et al. (2022c). The matching proportions, lengths, and thicknesses suggest that the models accurately replicate the geologically plausible meter-scale heterogeneity of the buildups as observed in the outcrop. The velocity and density models were constructed using facies as the common denominator. The properties (Figure 6d) were populated from laboratory-scale measurements of the outcrop core measured by Ramdani et al. (2022a). We assigned a constant value for facies to simplify the property models. For model 1, we assigned V_P = 4500 m/s, V_S = 2600 m/s, and density = 2.4 g/cm^3 to the buildups, and V_P = 2400 m/s, V_S = 1730 m/s, and density = 2.2 g/cm^3 to the background strata. For model 2, we assigned similar buildup properties and used V_P = 2252 m/s, V_S = 1350 m/s, and density = 2.1 g/cm^3 for the extended background strata. The resulting P-wave velocity models (Figure 6f) showcased the heterogeneity and velocity contrast between the buildups and the background strata.

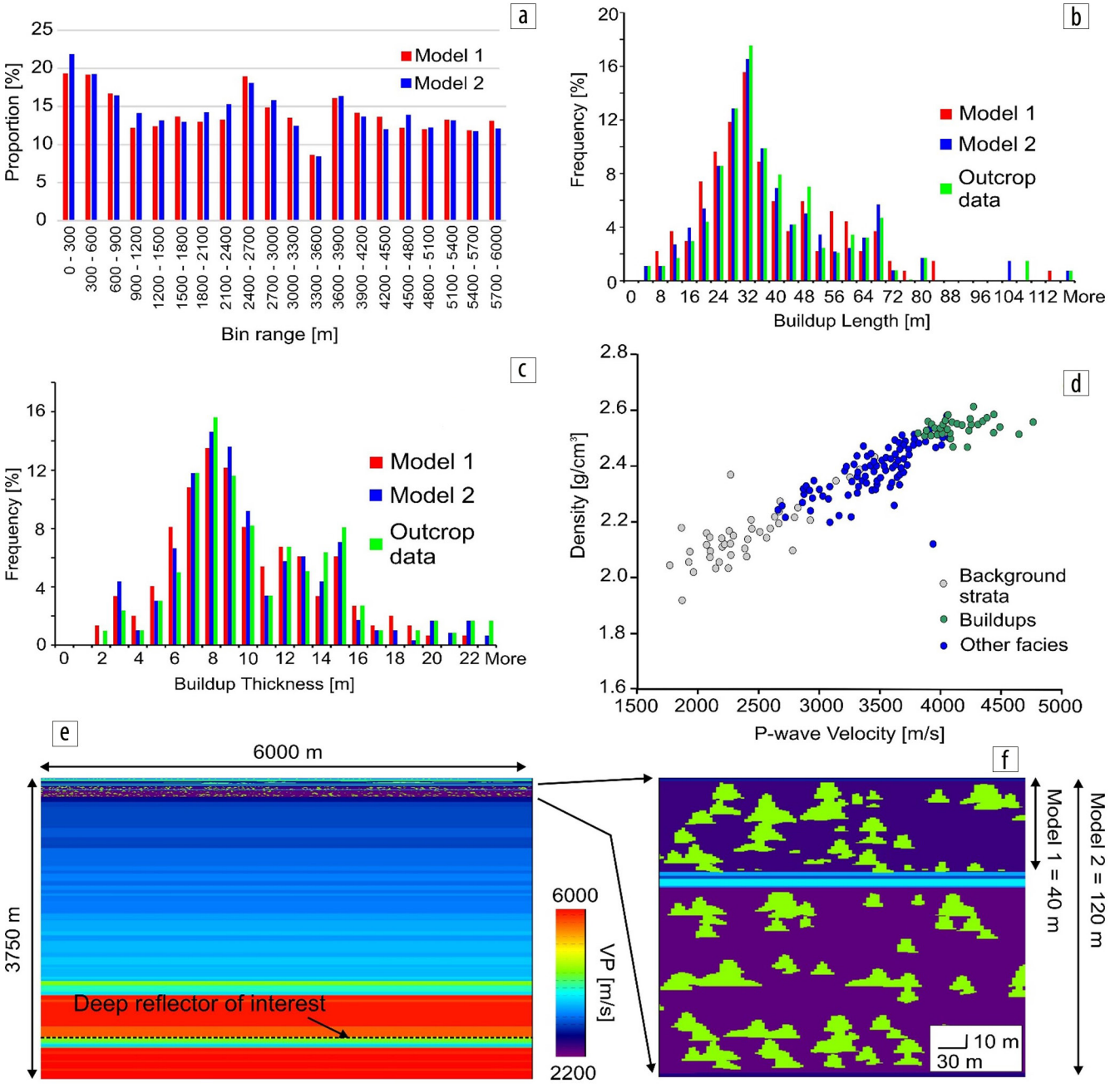

Figure 6. (a) The proportion of buildup facies calculated for 300 m length bins across the entire model. The buildups occupy approximately 10% to 20% of the strata, with an average proportion of about 14%. (b) The distribution of buildup lengths in the model as compared to the corresponding data observed in outcrops. (c) The distribution of buildup thicknesses in the models as compared to the corresponding data observed in outcrops (Ramdani et al., 2022c). The comparison reveals a high level of consistency between the models and the observed data, indicating their reliability. (d) A crossplot representing the relationship between P-wave velocity and density, with the color-coded facies from the outcrop core (Ramdani et al., 2022a). Notably, the P-wave velocity of the buildups appears to be nearly twice as high as that of the background strata. (e) An example of the entire P-wave velocity model with near-surface scattering layer at the top and horizontal layering below. (f) A zoomed-in view of the P-wave velocity model focusing specifically on the near-surface scattering layer with buildups. An arrow in (e) indicates a deep reflector of interest used for phase analysis.

DOI:10.1190/tle42100683.1

Synthetic seismic modeling and data assessment. As an initial step in this modeling study, we used a 1D model based on a velocity profile extracted from the SEAM Barrett model (Oristaglio, 2012). However, we substituted the near-surface layer with a newly constructed layer incorporating realistic geologic modeling of meter-scale heterogeneity, as described earlier (see Figure 6e). The resulting 2D model had dimensions of 6000 × 3750 m.

Finite-difference elastic modeling was conducted using a Klauder wavelet with a frequency range of 1.5 to 50 Hz. We computed 300 shot gathers with a 10 m spacing between shots, and the receivers had a split-spread geometry with a maximum offset of 1500 m and a spacing of 10 m.

To establish the relationships between the depicted models and the speckle noise mechanism shown in Figure 2, it is important to consider the connection between the elastic property heterogeneity and the scale of the seismic wave propagation. By examining a central frequency of 25 Hz, we find that the ratio of the wavelength (90 m) to the dominant thickness (8 m, Figure 6c) is approximately 11. For a maximum frequency of 50 Hz, this ratio is approximately 6. At a lower frequency of 10 Hz, the ratio expands to about 28.

These ratios confirm that the buildups primarily represent small-scale heterogeneity, consistent with the assumptions made in the speckle model presented in Figure 2. It is important to mention that we might find smaller wavelength-heterogeneity ratios when accounting for buildup length (Figure 6b), higher frequencies, thicker, or clustered buildups (as seen in Figure 5). It is essential to recognize that the seismic wavefield encompasses a broad range of frequencies, which presents an additional challenge that may not be encountered in other fields, such as optics and acoustics, where monochromatic or narrow-band measurements are more common.

Nevertheless, despite these challenges, we strove to accurately represent the geologic reality in our models and proceeded with a straightforward analysis under the assumption of predominantly small-scale heterogeneity. This approach allowed us to capture important aspects of the speckle noise mechanism while acknowledging the broader range of frequencies encountered in seismic data.

Figure 7a displays a typical common-shot gather obtained from a reference layered model, created by removing all buildups from model 1 (40 m buildup complex). The reflections in this model exhibit complete regularity, displaying consistent waveforms from trace to trace. Our analysis focuses on the deep reflector inside the ground roll cone, as indicated by the arrow in Figure 7. Both Figures 7b and 7c show comparable common-shot gathers, representing models 1 and 2, respectively. In Figure 7b, the prestack data already exhibit a characteristic speckled appearance, despite the buildups only occupying a relatively thin layer of 40 m (model 1), which is approximately 0.4 times the dominant P-wave wavelength. Figure 7c shows prestack data from model 2, where a 120 m thick heterogeneous near-surface layer is present. In this case, the speckled appearance is more pronounced, even though this layer represents only about 1.25 times the wavelength and is less than 4% of the total propagation distance between the surface and the deep reflector (at a depth of 3200 m).

We conclude that near-surface scattering layers containing stromatoporoid-coral buildup complexes exhibit characteristic distortions typically seen in hard-to-image field data from complex desert environments. The modeled distortions observed in Figures 7b and 7c resemble those seen in the real data shown in Figure 1, where the distortions are not limited to specific areas but spread throughout the gather, affecting first arrivals, ground roll, and reflections alike. While there is a common perception that certain near-surface imprints might "heal" as we go deeper, it is clear that speckle noise does not exhibit the same behavior. As the arrow in Figure 7 points out, even deep reflectors continue to show a cluttered pattern. Similar to how water droplets on a windshield can obscure the entire view, the near-surface heterogeneity, despite only occupying a small volume fraction of the section as a whole, can obscure the seismic gather from top to bottom.

The use of mathematical clutter as a substitute for the near-surface scattering layer (Bakulin et al., 2020, 2021, 2022) represented a meaningful advancement in the pursuit of a realistic "geologic clutter" model that accurately portrays the stromatoporoid-coral buildup. It is important to highlight that the statistical characteristics of the geologic clutter, such as the concentration of the buildups (Figure 6a), can exhibit consistency within specific geologic regimes. Thus, it is feasible to locally approximate the geologic clutter as a "random-like" heterogeneity, in line with the assumptions of speckle noise (Bakulin et al., 2022).

The distortions depicted in Figure 1 are not limited to isolated or exceptional common-shot gathers; rather, they persist over

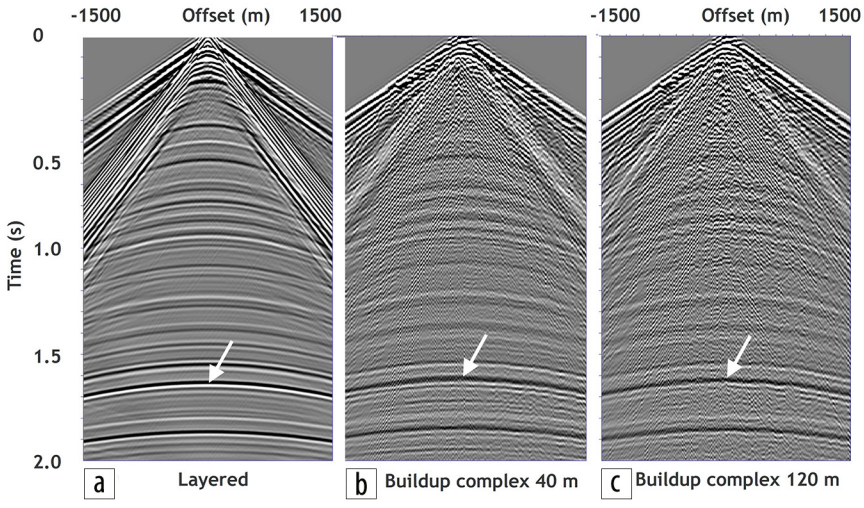

Figure 7. Representative common-shot gathers for each subsurface model: (a) the layered model; (b) the model with a near-surface scattering layer of 40 m thickness; and (c) the model with a near-surface scattering layer of 120 m thickness. The heterogeneous near-surface layers, as shown in Figures 5 and 6, create an escalating speckled appearance in (b) and (c), in contrast to the regular character of the layered model. The arrow identifies the deep reflector used for the phase analysis.

distances spanning tens of kilometers or more, which is in line with the expected extent of subsurface geologic features. In complex areas, field data may exhibit gradual lateral character variations attributable to geologic environment changes. These changes could stem from variations in the total thickness of the scattering formations, as well as variations in the concentration and/or thickness/length of the buildups (Figures 6a–6c).

Both the mathematical clutter and the geologic clutter models generate a similar speckled appearance in the synthetic seismic data with random phase perturbations, mirroring the observations made in field data. This further reinforces their usefulness as representative models.

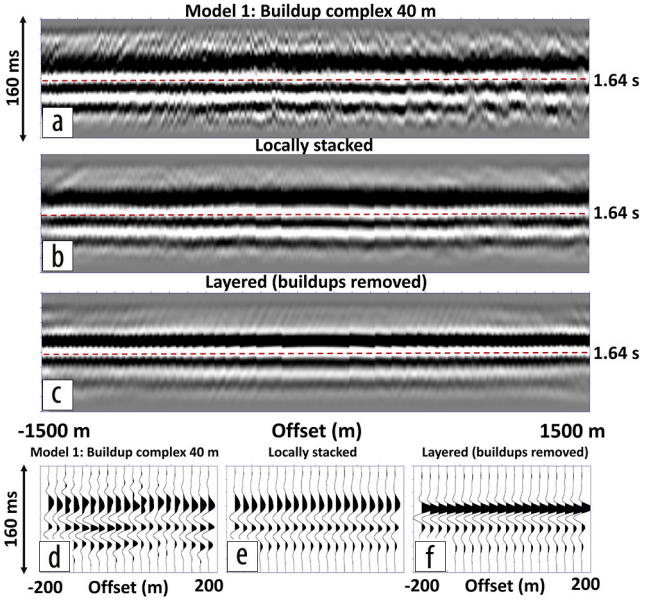

Figure 8. Time windows around deep reflector extracted from common-shot gathers in Figure 7 selected for phase analysis: (a) raw data for model 1 with a near-surface scattering layer of 40 m thickness; (b) locally stacked data of the same data from (a); (c) clean data in layered model with all buildups removed. Zooms into near-offset range [–200,200]m are shown in (d)–(f). Notably, we can observe distorted arrivals in panel (a)/(d), while the events after local stacking in panel (b)/(e) are much smoother, approaching the clean data in panel (c)/(f). It is worth noting that the reflector has been flattened by applying normal moveout corrections.

Phase analysis. Let us assess whether simulated gathers for geologically feasible near-surface heterogeneity comply with the multiplicative model equations 1–3 with random phase perturbations. We focus on the deep, strong reflector labeled in Figures 6 and 7. To calculate the local phase, we follow a similar procedure to the one used for real data in Figure 4.

First, we generated a locally stacked version from a dense 2D single-sensor acquisition. Rather than using nonlinear beamforming, we performed a simple supergrouping (Bakulin et al., 2018) of 30 neighboring common-offset traces collected over a 300 m aperture. Figure 8 depicts the time windows used to analyze model 1 with a 40 m buildup complex. When a near-surface scattering layer is present, the reflection events display jittery and speckle-like behavior, as shown in Figure 8a. The zoomed-in view in Figure 8d reveals that the jitteriness is not caused solely by simple time shifts but also by complex variations in the waveform from trace to trace. The locally stacked data (Figures 8b and 8e) exhibit much smoother behavior, approaching the clean data (Figures 8c and 8f), where all heterogeneities are removed. Thus, the locally stacked data can be conceptually considered a modified data set in a simplified model, where at least smaller-scale heterogeneities were either removed or smoothed out.

Figure 9 shows the distribution of residual phase obtained by computing the difference between the phase of raw and locally stacked data, using the same method as employed for the field data. The first major observation is that all phase deviations are quasi-normal in nature and approximately symmetric at about zero. This suggests that the phase variations randomly oscillate around the beamformed phase (i.e., phase of locally stacked data), exhibiting symmetry in both positive and negative directions consistent with the random noise model proposed. The second major observation is that the spread or standard deviation of the phase distribution increases at higher frequencies. This can be physically intuitive as fixed distributions of buildups are less disruptive to longer wavelengths (lower frequencies).

Figures 10 and 11 show the same analysis for model 2, which features a buildup complex spanning 120 m. In these figures, waveform distortions are stronger and demonstrate larger changes from trace to trace, despite the relatively tight receiver sampling of 10 m (compare Figures 10a and 8a, or 10d and 8d). This

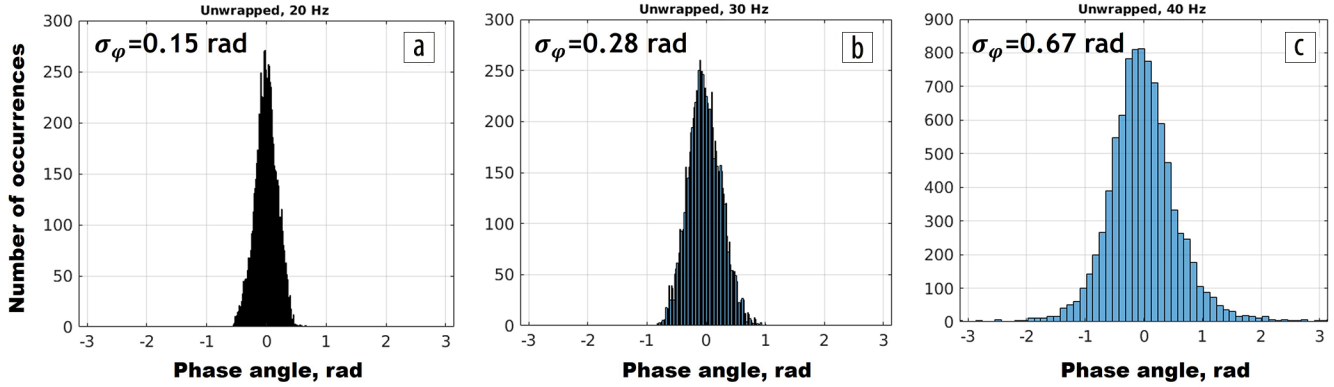

Figure 9. Histograms of the residual phase distribution at various frequencies, namely (a) 20 Hz, (b) 30 Hz, and (c) 40 Hz. The residual phase is obtained by calculating the difference in the wrapped phase between the raw data in Figure 8a and the locally stacked data in Figure 8b. The histograms reveal two key findings. First, we observe a quasi-normal distribution that is approximately symmetric around zero. Second, we can see that the distribution's spread or standard deviation increases with higher frequencies.

observation aligns with the mechanism portrayed in Figure 2. The increased thickness of the scattering layer gives rise to a broader range of forward-scattering near-ballistic arrivals, resulting in more intricate and rapidly varying interference patterns.

The histograms of the phase variations shown in Figure 11 support the visual observations regarding the more severe distortions, and have a wider spread or standard deviation at each frequency than in Figure 9 for model 1. Given the approximately similar concentration and geometry of the buildups in both model 1 and model 2 (Figures 6a–6c), the observed discrepancy in the spread between them indicates a clear dependence of phase perturbations on the thickness of the scattering layer. A larger thickness of the scattering layer leads to more pronounced phase perturbations. Further studies are required to gain a deeper insight into this relationship and to develop a comprehensive understanding of the underlying dynamics.

Despite the difference in the magnitude of phase perturbations, the same two main conclusions can also be drawn from model 2 as from model 1. First, the plots in Figure 11 exhibit a symmetric and near-Gaussian distribution of phase variations, indicating the quasi-random nature of the residual phase fluctuations. This finding holds for all the plots, further emphasizing the consistent character of the observed phase perturbations. Second, there is a noticeable increase in the spread or standard deviation as the frequency increases. This aligns with the experimental frequency-perturbation relationship in field data, emphasizing the frequency-dependent nature of the speckle noise model.

Considering both model 1 and model 2 together confirms the quasi-random nature of the residual phase and the frequency-dependent spread of perturbations.

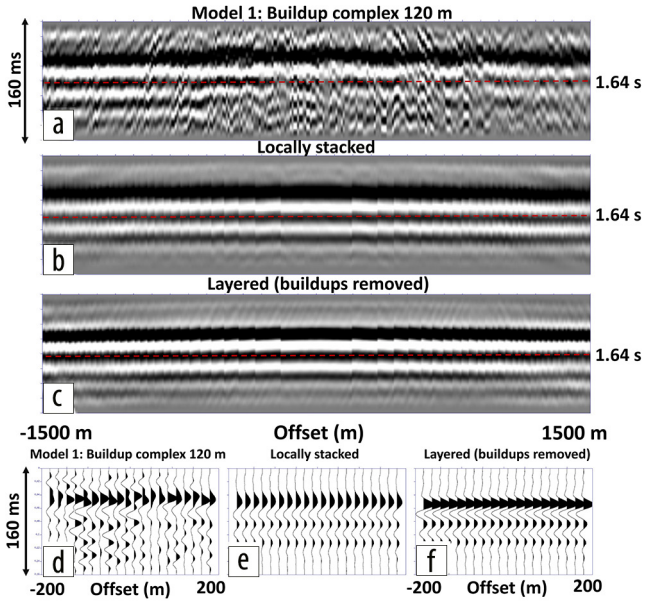

Figure 10. Same as Figure 8 but for model 2 with 120 m buildup complex. Observe more severe waveform distortions caused by thicker near-surface scattering layer.

Other potential geologic sources of speckle noise

We have shown how speckle noise may be attributed to meter-scale facies heterogeneity arising from the distribution, growth pattern, and property variations within the stromatoporoid-coral buildups. We acknowledge that these types of reefal geobodies are not exclusive to the occurrence of speckle noise. Similar heterogeneities have been observed in other geologic formations as well. For example, the Upper Cambrian microbial buildups in Texas (Khanna et al., 2020), terminal Proterozoic to Cambrian thrombolite-stromatolite reefs in Namibia (Adams et al., 2005), Aptian Lithocodium-Bacinella buildups in Oman (Rameil et al., 2010), and Albian rudists buildup in Texas (Janson et al., 2015) all exhibit comparable growth patterns to the buildup facies examined in our study. It is likely, therefore that the geologic origin of speckle noise may extend beyond the stromatoporoid-coral buildup alone.

Extensive research has documented various drastic (negative) impacts on seismic data of small-scale geologic heterogeneity in igneous rock, including intrusive (Eaton et al., 2003) and extrusive (Ziolkowski et al., 2003) formations. Reflection seismology tends to lag behind other geophysical methods when it comes to hard-rock environments. This is primarily due to intense scattering noise, which disrupts reflections to a greater extent compared to sedimentary basins. Ziolkowski et al. (2003) even proposed modifying the acquisition process to acquire preferentially lower frequencies in light of this challenge. This is primarily due to intense scattering noise, which disrupts reflections to a greater

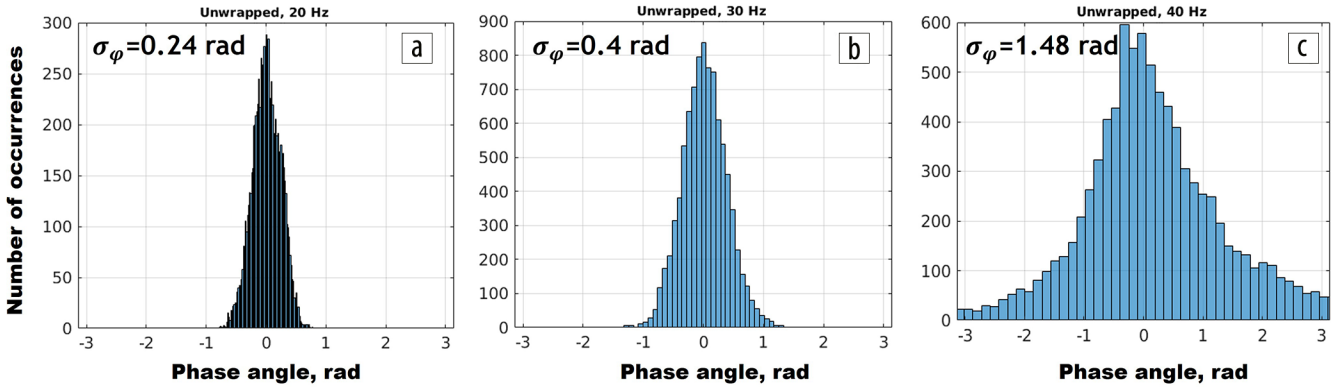

Figure 11. Same as Figure 9 but for model 2 with a 120 m buildup complex. Observe a more extensive spread at each frequency due to the increased thickness of the near-surface scattering layer compared to Figure 9. This greater spread emphasizes that the magnitude of phase variations is influenced not only by the sizes and distribution of heterogeneity (which remain consistent between model 1 and 2) but also by the thickness of the scattering layer.

extent than in sedimentary basins. They found that conventional methods employed at higher frequencies were ineffective in addressing the scattering noise issue. This is consistent with our findings suggesting weaker phase variations at lower frequencies. Hard-rock settings are gaining importance due to the renewed focus on critical minerals and geothermal energy.

To summarize, small-scale heterogeneity is widespread across various geologic settings, and a major breakthrough in enhancing seismic resolution could be achieved by effectively addressing speckle noise using novel workflows such as seismic time-frequency masking (Bakulin et al., 2023). Hence, it is crucial to comprehend and address speckle noise for various applications, including oil and mineral exploration, geothermal energy, and carbon storage monitoring.

Conclusions

In the realm of deep exploration, a central focus lies on thoroughly characterizing the velocities of near-surface and shallow overburden layers. The goal is to mitigate their adverse impacts on imaging target areas. This study examines scenarios where the near surface exhibits prominent concentrations of small-scale heterogeneities. As a result, the entire wavefield becomes cluttered or speckled, presenting challenges for efficient processing and imaging.

To address these issues, we introduce a speckle mechanism and noise model that reveal the reflection distortions arising from meter-scale near-surface scattering. We identify scattering noise as a propagation distortion arising from forward scattering on numerous small-scale heterogeneities. This noise resembles the well-known speckle noise observed in fields like optics and acoustics. Taking inspiration from these fields, a seismic speckle noise model has recently emerged — a multiplicative random noise model that involves random phase perturbations.

Our study constructs a realistic meter-scale geologic model for near-surface layers, effectively demonstrating their ability to create the distortions predicted by the speckle noise model. This demonstration holds crucial significance for several reasons. Firstly, it dispels the notion that the resolution of challenges in deep imaging solely revolves around refining the characterization of the superimposed near-surface noise to the extent that undistorted reflections from the targets become apparent upon its removal. We demonstrate that speckle noise is a multiplicative signal distortion and cannot be mitigated through subtraction. Secondly, it prompts a reevaluation of the concept of an "ideal" near-surface model that supposedly resolves all imaging complexities. Speckle noise investigations suggest that the pursuit of deterministic models to correct these distortions is an unattainable objective. The meter-scale variations responsible for speckle noise, as presented, remain unrecoverable even with advanced techniques for building velocity models due to their small size and complex interactions.

Most importantly, validating the multiplicative speckle noise model through real-world geologic heterogeneity at the meter scale establishes a foundation for effective statistical despeckling techniques. Notably, seismic time-frequency masking harnesses the full potential of the random multiplicative noise model to eliminate detrimental scattering distortions from prestack data. This strategy capitalizes on insights from speckle noise studies and the multiplicity (fold) of prestack seismic data. As a result, phase and amplitude corrections are meticulously guided by information derived from locally stacked data.

Through a comparison of phase perturbations in both real-world and synthetic data, we establish similarities in their fundamental statistical properties. The phase perturbations resulting from small-scale scattering exhibit a quasi-random nature and adhere to a nearly normal distribution. This observation holds true for both 40 and 120 m buildup complexes. Additionally, we find that increasing the thickness of the near-surface scattering layer leads to more pronounced reflection distortions and a wider range of phase perturbations. Therefore, the statistical characteristics of speckle noise are influenced by the geometric and elastic properties of the buildup layers and the overall thickness of the accommodating scattering layer.

Furthermore, we observe that the spread or standard deviation of phase perturbations increases with frequency in both real-world and synthetic data. This observation holds significant implications, potentially accounting for the loss of higher frequencies during local or global stacking in processing. While residual statics only address the kinematic aspect of the complex wavefield perturbation stemming from small-scale near-surface variations, it falls short of fully resolving the problem. In contrast, the speckle noise model effectively captures the intricate waveform distortion caused by frequency-dependent phase perturbations. This model forms the fundamental basis for emerging advanced techniques like seismic time-frequency masking, which are designed to correct reflection distortions. These innovative methods, known as despeckling or decluttering, introduce new processing tools.

Drawing insights from other disciplines to tackle speckle noise could significantly accelerate our progress in this field. Effectively managing frequency-dependent speckle distortions in broadband seismic data represents the next significant step in improving seismic imaging in complex near-surface or overburden conditions. TLE

Acknowledgments

We thank current and previous Saudi Aramco colleagues Philip Thomson, Yazki Ibrahim, and Simon Cordery for providing the various data examples shown.

Data and materials availability

Data associated with this research are confidential and cannot be released.

Corresponding author: a_bakulin@yahoo.com

References

Adams, E. W., J. P. Grotzinger, W. A. Watters, S. Schröder, D. S. McCormick, and H. A. Al-Siyabi, 2005, Digital characterization of thrombolite-stromatolite reef distribution in a carbonate ramp system (terminal Proterozoic, Nama Group, Namibia): AAPG Bulletin, **89**, no. 10, 1293–1318, https://doi.org/10.1306/06160505005.

Ait-Messaoud, M., M. Boulegroun, A. Gribi, R. Kasmi, M. Touami, B. Anderson, P. Van Baaren, et al., 2005, New dimensions in land seismic technology: Schlumberger Oilfield Review, **17**, 42–53.

Al-Mojel, A., P. Razin, and G. Dera, 2020, High-resolution sedimentology and sequence stratigraphy of the Oxfordian-Kimmeridgian, Hanifa, Jubaila and Arab outcrops along Jabal Tuwaiq, Central Saudi Arabia: Journal of African Earth Sciences, **165**, 103803, https://doi.org/10.1016/j.jafrearsci.2020.103803.

Bakulin, A., P. Golikov, M. Dmitriev, V. Dolgov, and D. Neklyudov, 2016, Application of supergrouping to land seismic data in desert environment: 86th Annual International Meeting, SEG, Expanded Abstracts, 4649–4653, https://doi.org/10.1190/segam2016-13838765.1.

Bakulin, A., P. Golikov, M. Dmitriev, D. Neklyudov, P. Leger, and V. Dolgov, 2018, Application of supergrouping to enhance 3D prestack seismic data from a desert environment: The Leading Edge, **37**, no. 3, 200–207, https://doi.org/10.1190/tle37030200.1.

Bakulin, A., D. Neklyudov, and I. Silvestrov, 2021, Targeted noise removal by seismic time-frequency masking (STFM) and minimum statistics approach: First International Meeting for Applied Geoscience & Energy, SEG/AAPG, Expanded Abstracts, 2879–2884, https://doi.org/10.1190/segam2021-3581846.1.

Bakulin, A., D. Neklyudov, and I. Silvestrov, 2022, Multiplicative random seismic noise caused by small-scale near-surface scattering and its transformation during stacking: Geophysics, **87**, no. 5, V419–V435, https://doi.org/10.1190/geo2021-0830.1.

Bakulin, A., D. Neklyudov, and I. Silvestrov, 2023, Seismic time-frequency masking for suppression of seismic speckle noise: Geophysics, **88**, no. 5, V371–V385, https://doi.org/10.1190/geo2022-0779.1.

Bakulin, A., D. Neklyudov, and I. Silvestrov, 2020, Prestack data enhancement with phase corrections in time-frequency domain guided by local multidimensional stacking: Geophysical Prospecting, **68**, no. 6, 1811–1818, https://doi.org/10.1111/1365-2478.12956.

Bakulin, A., and I. Silvestrov, 2021, Understanding acquisition and processing challenges in the desert environment through SEAM Arid and Barrett models: 91th Annual International Meeting, SEG, Expanded Abstracts, 2824–2829.

Bakulin, A., I. Silvestrov, M. Dmitriev, D. Neklyudov, M. Protasov, K. Gadylshin, V. Tcheverda, and V. Dolgov, 2018, Nonlinear beamforming for enhancing prestack seismic data with a challenging near surface or overburden: First Break, **36**, no. 12, 121–126, https://doi.org/10.3997/1365-2397.n0143.

Borgomano, J., J.-P. Masse, M. Fenerci-Masse, and F. Fournier, 2013, Petrophysics of Lower Cretaceous platform carbonate outcrops in Provence (SE France): Implications for carbonate reservoir characterization: Journal of Petroleum Geology, **36**, no. 1, 5–41, https://doi.org/10.1111/jpg.12540.

Bridle, R., N. Barsoukov, M. Al-Homaili, R. Ley, and A. Al-Mustafa, 2006, Comparing state-of the art near-surface models of a seismic test line from Saudi Arabia: Geophysical Prospecting, **54**, no. 6, 667–680, https://doi.org/10.1111/j.1365-2478.2006.00564.x.

Cary, P. W., and G. A. Lorentz, 1993, Four-component surface-consistent deconvolution: Geophysics, **58**, no. 3, 383–392, https://doi.org/10.1190/1.1443421.

Cordery, S., 2020, An effective data processing workflow for broadband single-sensor single-source land seismic data: The Leading Edge, **39**, no. 6, 401–410, https://doi.org/10.1190/tle39060401.1.

Dmitriev, M., A. Bakulin, and P. Golikov, 2017, Efficient four-dimensional supergrouping algorithm for enhancement of high-channel count seismic data: 87th Annual International Meeting, SEG, Expanded Abstracts, 4986–4990, https://doi.org/10.1190/segam2017-17668141.1.

Eaton, D. W., B. Milkereit, and M. H. Salisbury, eds., 2003, Hardrock seismic exploration: SEG, https://doi.org/10.1190/1.9781560802396.

Eberli, G. P., G. T. Baechle, F. S. Anselmetti, and M. L. Incze, 2003, Factors controlling elastic properties in carbonate sediments and rocks: The Leading Edge, **22**, no. 7, 654–660, https://doi.org/10.1190/1.1599691.

Goodman, J. W., 2020, Speckle phenomena in optics: Theory and applications, 2nd ed.: SPIE Press, https://doi.org/10.1117/3.2548484

He, B., X.-B. Xie, H. Ning, Y. He, and B. Chen, 2017, The effect of strong near-surface scattering on the quality of seismic imaging: 87th Annual International Meeting, SEG, Expanded Abstracts, 2715–2720, https://doi.org/10.1190/segam2017-17654529.1

Janson, X., K. Lee, C. Zahm, and K. Kerans, 2015, Ground-penetrating radar imaging of Albian rudist buildups, central Texas: Interpretation, **3**, no. 3, SY67–SY81, https://doi.org/10.1190/INT-2014-0273.1.

Khanna, P., M. Pyrcz, A. W. Droxler, H. H. Hopson, P. M. Harris, and D. J. Lehrmann, 2020, Implications for controls on Upper Cambrian microbial build-ups across multiple-scales, Mason County, Central Texas, USA: Marine and Petroleum Geology, **121**, 104590, https://doi.org/10.1016/j.marpetgeo.2020.104590.

Oristaglio, M., 2012, SEAM Phase II—Land Seismic Challenges: The Leading Edge, **31**, no. 3, 264–266, https://doi.org/10.1190/1.3694893.

Ramdani, A., V. Chandra, T. Finkbeiner, and V. Vahrenkamp, 2023, Multi-scale geophysical characterization of microporous carbonate reservoirs utilizing machine learning techniques: An analog case study from an Upper Jubaila Formation outcrop, Saudi Arabia: Marine and Petroleum Geology, **152**, 106234, https://doi.org/10.1016/j.marpetgeo.2023.106234.

Ramdani, A., P. Khanna, T. Adigozalova, G. S. Gairola, and V. Vahrenkamp, 2022a, Near-surface core data from the Late Jurassic Hanifa Fm outcrop — Wadi Birk, Central Saudi Arabia: Shallow marine carbonate platform sediments equivalent to Arabian subsurface reservoirs: Mendeley Data, V1, https://doi.org/10.17632/3dbx4tgv9s.1.

Ramdani, A., P. Khanna, S. de Jong, G. S. Gairola, and V. Vahrenkamp, 2022b, How in-place volumes of subsurface reservoir models are impacted by using 3D high-resolution outcrop analogue data. A case study using depositional architectural heterogeneity of stromatoporoid/coral buildups of the Hanifa Fm, Saudi Arabia: International Petroleum Technology Conference, paper no. IPTC-21878-MS, https://doi.org/10.2523/IPTC-21878-MS.

Ramdani, A., P. Khanna, S. De Jong, G. S. Gairola, S. Hanafy, and V. Vahrenkamp, 2022c, Three-dimensional morphometric analysis and statistical distribution of the Early Kimmeridgian Hanifa Formation stromatoporoid/coral buildups, central Saudi Arabia: Marine and Petroleum Geology, **146**, 105934, https://doi.org/10.1016/j.marpetgeo.2022.105934.

Rameil, N., A. Immenhauser, G. Warrlich, H. Hillgärtner, and H. J. Droste, 2010, Morphological patterns of Aptian Lithocodium–Bacinella geobodies: Relation to environment and scale: Sedimentology, **57**, no. 3, 883–911, https://doi.org/10.1111/j.1365-3091.2009.01124.x.

Stork, C., 2020, How does the thin near surface of the earth produce 10–100 times more noise on land seismic data than on marine data?: First Break, **38**, no. 8, 67–75, https://doi.org/10.3997/1365-2397.fb2020062.

Vahrenkamp, V., P. Khanna, A. Petrovic, A. Ramdani, G. S. Gairola, I. Putri, and A. Sorrentino, 2019, Integrated workflows for characterizing reservoir heterogeneities with ancient and modern carbonate outcrop analogues: Abu Dhabi International Petroleum Exhibition and Conference, paper no. SPE-197851-MS, https://doi.org/https://doi.org/10.2118/197851-ms.

Vesnaver, A., 2006, Near-surface challenges and advances in the Arabian Peninsula: Geophysical Prospecting, **54**, no. 6, 663–664, https://doi.org/10.1111/j.1365-2478.2006.00571.x.

Ziolkowski, A., P. Hanssen, R. Gatliff, H. Jakubowicz, A. Dobson, G. Hampson, X.-Y. Li, and E. Liu, 2003, Use of low frequencies for sub-basalt imaging: Geophysical Prospecting, **51**, no. 3, 169–182, https://doi.org/10.1046/j.1365-2478.2003.00363.x.